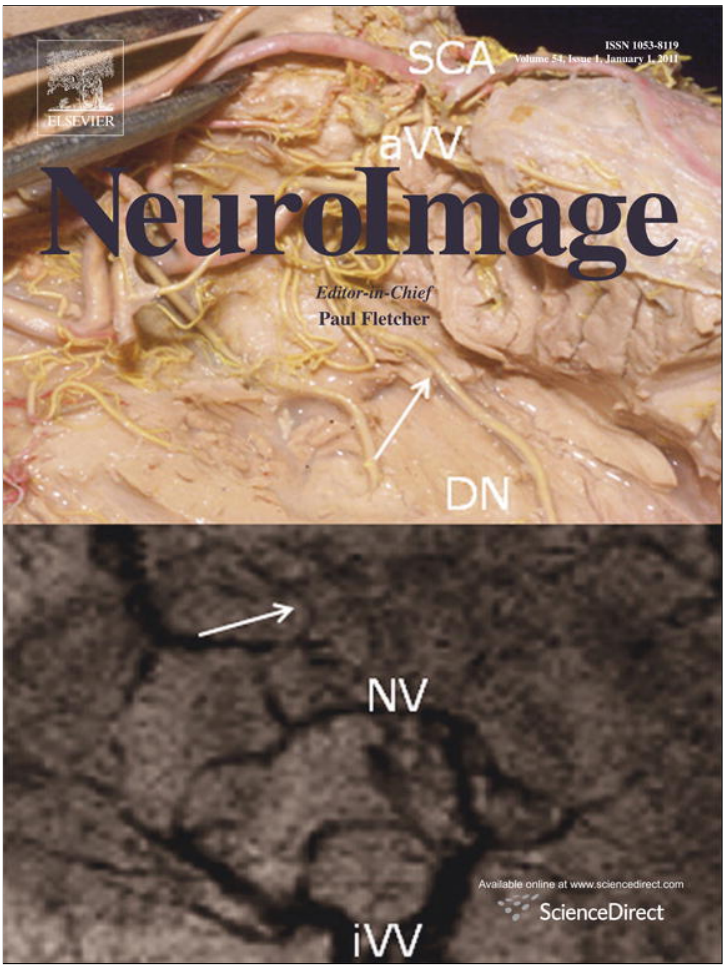

(This is a sample cover image for this issue. The actual cover is not yet available at this time.)

NeuroImage 59 (2012) 3297–3308

Contents lists available at SciVerse ScienceDirect

NeuroImage

journal homepage: www.elsevier.com/locate/ynimg

3D Statistical Parametric Mapping of quiet sleep EEG in the first year of life ☆

Jorge Bosch-Bayard [a,*], Pedro A. Valdés-Sosa [a], Thalía Fernandez [b], Gloria Otero [c], Bernardo Pliego Rivero [c], Josefina Ricardo-Garcell [b], Berta González-Frankenberger [b], Lídice Galán-García [a], Antonio Fernandez-Bouzas [b], Eduardo Aubert-Vazquez [a], Agustin Lage-Castellanos [a], René Rodríguez-Valdés [a], Thalía Harmony [b]

[a] Centro de Neurociencias de Cuba, Avenida 25 y 158, Playa, La Habana, Cuba
[b] Departamento de Neurobiología Conductual y Cognitiva, Instituto de Neurobiología, Universidad Nacional Autónoma de México, Campus Juriquilla, Queretaro, Mexico
[c] Facultad de Medicina, Universidad Autónoma del Estado de México, Toluca, Mexico

ARTICLE INFO

Article history:
Received 28 April 2011
Revised 12 October 2011
Accepted 1 November 2011
Available online 10 November 2011

Keywords:
Infants
Source analysis
EEG norms
VARETA
LORETA
SPM

ABSTRACT

This paper extends previously developed 3D SPM for Electrophysiological Source Imaging (Bosch et al., 2001) for neonate EEG. It builds on a prior paper by our group that established age dependent means and standard deviations for the scalp EEG Broad Band Spectral Parameters of children in the first year of life. We now present developmental equations for the narrow band log spectral power of EEG sources, obtained from a sample of 93 normal neonates from age 1 to 10 months in quiet sleep. The main finding from these regressions is that EEG power from 0.78 to 7.5 Hz decreases with age and also for 45–50 Hz. By contrast, there is an increase with age in the frequency band of 19–32 Hz localized to parietal, temporal and occipital areas. Deviations from the norm were analyzed for normal neonates and 17 with brain damage. The diagnostic accuracy (measured by the area under the ROC curve) of EEG source SPM is 0.80, 0.69 for average reference scalp EEG SPM, and 0.48 for Laplacian EEG SPM. This superior performance of 3D SPM over scalp qEEG suggests that it might be a promising approach for the evaluation of brain damage in the first year of life.

Introduction

In this paper we present 3D source EEG Statistical Parametric Mapping (SPM) and norms for quiet sleep in the first year of life. This is an extension of an earlier paper (Bosch-Bayard et al., 2001) which introduced norms for 3D EEG source imaging for ages 5–97. In that paper we also described a type of Statistical Parametric Map (SPM) obtained by applying the z transform (with respect to the norm) to each source voxel. The use of this technique for imaging the electrophysiological consequences of brain disorders was also illustrated. At that time it was not possible to extend the norms to earlier ages due to the lack of (scalp) EEG databases and probabilistic brain atlases for that age range. The present paper remedies this situation using an appropriate data set and new methods.

In order to better explain our aims it is useful to summarize some relevant work in quantitative EEG interpretation (a more extensive review may be found in Hernandez-Gonzalez et al., 2011).

In spite of the electroencephalogram (EEG) being one of the most noninvasive, inexpensive and useful technique for assessing brain dysfunction it is still evaluated mainly by visual inspection (Scher, 2005; Schomer and Lopes da Silva, 2011). This is, unfortunately, a highly specialized skill with relatively low inter-evaluator reliability. This has spurred research since the 70's (Gevins and Remond, 1987) to develop more objective quantitative EEG analysis (qEEG) methods for use with both spontaneous EEG as well as Event Related Potentials (ERPs). An essential first step of these methods is the extraction of *descriptive parameters* (DP) that summarize clinically relevant features of the EEG. An important set of these DPs has been the spectral energy in either broad (John et al., 1977; Matousek and Petersén, 1973) or in narrow (Szava et al., 1994; Valdes et al., 1992) frequency bands.

A convenient tool for assessing abnormality is the statistical comparison of the DPs of a particular subject with regard to a normative data (John et al., 1977) especially by means of SPM (Galan et al., 1994; Huizenga et al., 2007), thus allowing the classification of the EEG of a given subject as belonging or not to the normal range taking covariates such as age into account. This approach has proven to be useful as a complement to visual inspection of the EEG in evaluating neurological and psychiatric disorders (Cantor and Chabot, 2009; Fernandez-Bouzas et al., 1995; Harmony et al., 1993). Double blinded ROC analyses of diagnostic accuracy of scalp EEG SPM procedures are described in Hernandez-Gonzalez et al. (2011). Obviously the performance of this type of SPM is contingent on the existence of the

☆ Dedication: We want to honor the memory of Prof. E. Roy John who not only initiated our group's work in qEEG but who was a great inspiration to us for decades. His presence is sorely missed.

* Corresponding author at: Cuban Neuroscience Center, Av. 25 y 158, Cubanacan, Havana, Cuba. Fax: +53 7 2086321.
E-mail addresses: bosch@cneuro.edu.cu, oldgandalf@yahoo.com (J. Bosch-Bayard).

1053-8119/$ – see front matter © 2011 Elsevier Inc. All rights reserved.
doi:10.1016/j.neuroimage.2011.11.001

appropriate EEG norms for different ages. It is therefore not surprising that a number of groups have carried out normative studies (e.g. Alvarez et al., 1987; Harmony et al., 1990; John et al., 1980, 1987; Matousek and Petersén, 1973; Szava et al., 1994; Valdes et al., 1992).

In spite of these promising results, this type of SPM was initially limited to DPs for *topographic* (scalp) EEG with a consequent poor spatial resolution. The development of Electrophysiological source Imaging (*ESI*) (reviewed in Michel et al., 2004) provided better 3D spatial resolution originating a *tomographic* version of qEEG. For more extensive reviews of this active area of research see Sekihara and Nagarajan (2008); Michel et al. (2009) and Valdes-Sosa et al. (2009). The natural extension of SPM from topographic to tomographic qEEG DPs was first described in Bosch-Bayard et al. (2001). Interestingly, 3D EEG source SPM not only provided higher spatial resolution but also greater diagnostic accuracy as measured with ROC curves (Hernandez-Gonzalez et al., 2011). It should be stressed that these results were obtained with a population based probabilistic MRI brain atlas instead of each subject's individual MRI in order to ensure wider clinical applicability.

As with the (scalp) EEG in older subjects, there is a long tradition of the clinical use of visually inspected EEG for neonates (Amzica and Lopes da Silva, 2011; Fenichel, 2007; Mizrahi et al., 2011; Riviello et al., 2011). For the same reasons mentioned above there has also been much work on trying to introduce topographic qEEG methods for this type of subject, especially in the context of neonatal monitoring (Hellström-Westas et al., 2008). An important part of this type of work has been the construction of normative databases. An early example is Hagne et al. (1973), followed by Joseph et al. (1976); Korotchikova et al.(2009); Mandelbaum et al. (2000); Niemarkt et al. (2010); Okumura et al. (2006); Paul et al. (2006); Victor et al. (2005); West et al. (2006); Willekens et al. (1984). Also several full age range normative databases (Gordon et al., 2005; Hunter et al., 2005; Thatcher et al., 1987) have also included neonates.

It should be noted that many of the cited studies on resting state EEG have been focused on stage 2 neonate of sleep (quiet sleep). This is understandable for several practical reasons: 1) It is easier to collect data without artifacts during sleep than during awaking in infants; 2) quiet sleep or sleep stage 2 is characterized by presenting sleep spindles, vertex waves and K complex that allow easier recognition during visual EEG inspection and edition when selecting data for qEEG processing, and 3) when infants fall asleep they transit directly to sleep stage 2 (Riviello et al., 2011). We also selected stage 2 as the focus of our study in a previous study in which we reported normative equations for broad band frequency analysis of the EEG background activity in a group of infants during the first year of life (Otero et al., 2011). The main findings were that delta and theta power decreases with age whereas alpha and beta increased.

It should be clear by now that the remaining step in the qEEG analysis of Stage 2 neonate sleep is to obtain tomographic norms for this type of EEG background activity as an extension of Bosch-Bayard et al. (2001) and to assess their usefulness in evaluating brain disorders in the first year of life. This work is precisely what is described in this paper.

This paper is organized in the following manner. In the Materials and methods section several specific data processing problems are addressed. One major issue is the rapid variation of brain anatomy for the first year of life which requires the use of age dependent forward models for the EEG in order to obtain valid EEG source spectra. The construction of probabilistic brain atlases for this age range (Fonov et al., 2011) greatly facilitated obtaining age dependent inverse solutions and is here described. A short summary of tomographic qEEG is then given for reference purposes. Special attention is given to the selection of the sample size in order for the norms to be representative of the infant population. The Results and discussion section then presents a quantitative description of the maturation of current source density spectra of the background EEG for quiet sleep at frequencies from 0.78 to 50 Hz in infants from 1 to 10 months of age. Data supporting the validity of the normative database is also given. The diagnostic accuracy of the 3D SPM maps is evaluated with a sample of newborns with brains disorders. Finally conclusions are drawn.

Materials and methods

Participants

The sample consisted of 93 infants (51 male, 42 female) from 1 to 10 months of age from two states in the central region of Mexico with a mean age of 5.16 months ($\pm$2.34). The age range was stratified to guarantee larger sample at earlier ages when brain changes accelerate (Table 1).

The inclusion criteria for normality were:

1. Normal delivery at term.
2. Weight at birth between 2500 g and 3900 g.
3. Apgar $\geq$8 at the first minute and $\geq$9 at the 5th minute after birth.
4. With no antecedents of pre or perinatal risk factors for brain damage.
5. Normal neurological and pediatric examination results.
6. Physical and mental development within normal limits (Bayley Scales of infant development) (Bayley, 1993).

EEG recordings

Twenty minutes of EEG recordings were in a dim lit and soundproofed room with infants remaining on the mother's lap. Electrodes were placed according to the 10–20 International System: Fp1, Fp2, F3, F4, C3, C4, P3, P4, O1, O2, F7, F8, T3, T4, T5, T6, Fz, Cz, Pz by means of a polyester cap (ElectroCap, International Inc., Eaton, Ohio), with linked ear lobes as a reference. Electrode impedances were considered acceptable if less than 5000 Ω. Simultaneously EKG and EMG were also recorded. Data was acquired using a digital electroencephalograph Medicid 4 System (Neuronic Mexicana, S.A., México) with differential amplifiers and gain of 10,000. The band pass was 0.3–100 Hz and 60 Hz notch, noise 2 microvolts RMS, and sample period of 5 ms.

The obtained data was edited offline. For analysis, 24–26 artifact-free segments, each of 2.56 s, were visually selected, thus guaranteeing that estimated cross-spectral matrices be positive definite, a necessary condition for qEEG analysis. An experienced neurophysiologist selected only windows in sleep stage 2 (Scher, 2005). Segments with artifacts or transient activity, sleep spindles, vertex waves or K complexes were discarded.

Transformation to the frequency domain

Following the methodology introduced in Bosch-Bayard et al. (2001), VARETA in the frequency domain (fdVARETA), was used to obtain an estimator of the EEG spectra at the sources of the brain electrical activity from the EEG voltage recorded at the scalp leads. VARETA is an Electrophysiological Source Imaging (ESI) method. Like LORETA (Pascual-Marqui, 2002; Pascual-Marqui et al., 1994)

Table 1
Mean and standard deviation of the sample ages. The sample was stratified in three groups of age to guarantee greater representation of lower ages in the sample, where the EEG and the brain size are changing faster.

Age range	Number of subjects	Mean age (months)	Std
$\leq$4.2 months	42	2.99	0.53
$>$4.2 and $\leq$7.2 months	32	6.20	0.60
$>$7.2 months	19	8.90	0.51
Total	93	5.16	2.34

VARETA is a Discrete Spline Distributed Solution (Riera et al., 1996). However, while LORETA imposes maximal spatial smoothness, VARETA imposes different amounts of spatial smoothness for different types of generators, the actual degree of smoothness in each voxel being data driven. VARETA eliminates "ghost solutions" (artifactual interference patterns), which are often present in linear distributed inverse solutions (Lutkenhoner et al., 2000). Recent surveys of the use of different types of ESI solutions in qEEG have recently been published (Hernandez-Gonzalez et al., 2011; Valdes-Sosa et al., 2009). Applications of VARETA and LORETA to the study of neurological (Fernandez-Bouzas et al., 2001) and psychiatric (Fernandez et al., 2007; Pascual-Marqui et al., 1999; Ricardo-Garcell et al., 2009) disorders, as well as for psychophysiological studies (Lehmann et al., 2006) have shown its validity for the study of these brain processes.

The Frequency domain version of VARETA (fdVARETA) is as follows:

a) Selected EEG epochs were transformed to the Average Reference.
b) Re-referenced EEG data was transformed to the frequency domain by means of the FFT and cross-segment averaging. Cross spectral matrices were calculated for every 0.39 Hz from 0.78 to 50 Hz. Spectral estimates were log-transformed in order to achieve approximate Gaussian distribution.
c) A Global Scale Factor (GSF) (Hernandez et al., 1994) was obtained from the spectral matrices and was applied to normalize the power spectra. The GSF is specific for each individual and accounts for the individual differences in power values due to skull thickness, hair volume, electrode impedance and other factors of variance of the EEG amplitude, not related to the electrophysiology.
d) Cross-spectral matrices at each frequency were used to calculate the source spectra for tomography (as described in the next section).

Estimation of the EEG spectra at the sources

In the Bosch-Bayard et al. (2001) paper the head and brain model necessary to solve the EEG forward problem was based on the Montreal Neurological Institute (MNI) brain template (Evans et al., 1993). As pointed out by one of the reviewers this brain template is not adequate for the first year of life. In order to obtain adequate EEG forward problem models, we used the age dependent brain templates created by V. Fonov at the MNI (Fonov et al., 2011), publicly available at http://www.bic.mni.mcgill.ca/ServicesAtlases/NIHPD-obj1.

Unfortunately, at present there is no parcellation of the infant brain, however this is work in progress,[1] and a more precise identification using IBASPM (Alemán-Gómez et al., 2006) will be possible in the near future.

Four templates were used: 0–2; 2–5; 5–8 and 8–11 months of age. Fig. 1 illustrates a representative T1 axial view for these four templates. In the first row, note the change in the intensity of the white matter from one template to the next. In the first two templates, the distribution of white matter intensity values overlaps with that of gray matter, making automatic tissue segmentation difficult. Therefore, segmentation of the gray matter for these templates was obtained by a semiautomatic procedure. For this same reason, it was not possible to calculate the forward model using realistic geometry since models failed either with Finite or Boundary Element Methods. Instead, using the aforementioned templates, an age dependent three concentric spheres model was used. The spherical model has significantly greater localization errors (3 cm on average) than more sophisticated model that warps the template to fiducial markers on the subject's head (0.8 cm on average) as described in Darvas et al. (2006). Nevertheless it was felt that it could provide a coarse localization of EEG sources that could later be refined in subsequent studies. For example the new methods described in Valdes-Hernandez et al. (2009), such as the Average Lead Field, could decrease the localization error even more but have yet to be adapted to the aforementioned difficulties in evaluating newborn MRIs.

The most important factors considered when creating the age dependent spherical EEG forward model for neonates were:

1. Change of head size: Fonov's methodology co-registers all brain templates to the same size. We correct for this by modeling the differences between infants' head size by assuming percent of increments of 4% from 0–2 to 2–5 months, 3% from 2–5 to 5–8 months and 2% from 5–8 to 8–11 months.
2. Changes in skull thickness and conductivity: When setting the conductivity of the different compartments of the spherical model in adults it has been common to use 1 for the brain tissue, 1/80 for the skull and 1 for the scalp (Homma et al., 1995; Rush and Driscoll, 1968). Lai et al. (2005) have estimated a more realistic conductivity value for the skull as 1/25 instead of 1/80. Oostendorp et al. (2000) have even proposed a value of 1/15. We are not aware of any study establishing the skull conductivity for the first year of life, but it is well known that the skull conductivity in infants is higher than in adults. Based on that evidence we assumed the 1/25 value for the conductivity of the adult skull and tentatively established the following rates for the infants' brain: 1:1/15:1 (for 0–2 months), 1:1/17:1 (for 2–5 months), 1:1/20:1 (for 5–8 months) and 1:1/23:1 (for 8–11 months).
3. Changes in the cortical gray matter mask: A grid over the gray matter was defined with a voxel size of $3\times3\times3$ mm (see Fig. 1, second row). According to the thickness of the gray matter of each template, a different number of sources were obtained for each of them. For the purpose of this paper, we selected the subset of sources that were common to all templates. The total number of sources produced by this procedure was 7368.

Thus using a spherical model that varied in size and conductivity for each age as well as varying cortical grid, the Lead Field matrices of the EEG forward problem were calculated for each template. The main factors involved in this computation are shown in the third row of Fig. 1, for a representative axial slice.

The resultant age dependent lead fields were used to estimate the source spectra for the 93 infants in the normative database, analyzed for each of the 127 frequencies, in steps of 0.39 Hz from 0.78 to 50 Hz. In order to restrict the permitted gradients from voxel to voxel and thereby specify the amount of smoothing, a "regularization parameter" must be calculated (Pascual et al., 1994). The regularization parameter calculated from the raw EEG cross-spectra of the normative subjects varied considerably. A major question was whether to calculate individual regularization parameters. However, after transformation to the average reference and rescaling to standardize the geometric power with the Global Scale Factor (Hernandez et al., 1994), the log of the regularization parameter was well described by a Gaussian distribution with mean 0.0222 and standard deviation 0.0061. In view of this small value for the standard deviation, the regularization parameter was fixed to the mean value. This accelerated the calculations by an order of magnitude.

Regression equations

Polynomial regressions were fitted to the log of the EEG spectra at all leads and sources. Thus age regression equations were calculated for the full frequency range (from 0.78 Hz to 50 Hz with a frequency resolution of 0.39 Hz) and age range (from 1 to 10 months), for the normative database.

Infant EEGs have a large inter-individual variability due to factors such as brain maturation, changes in the scalp conductivity and

[1] A. Evans & L. Collins, *Montreal Neurological Institute*, personal communication.

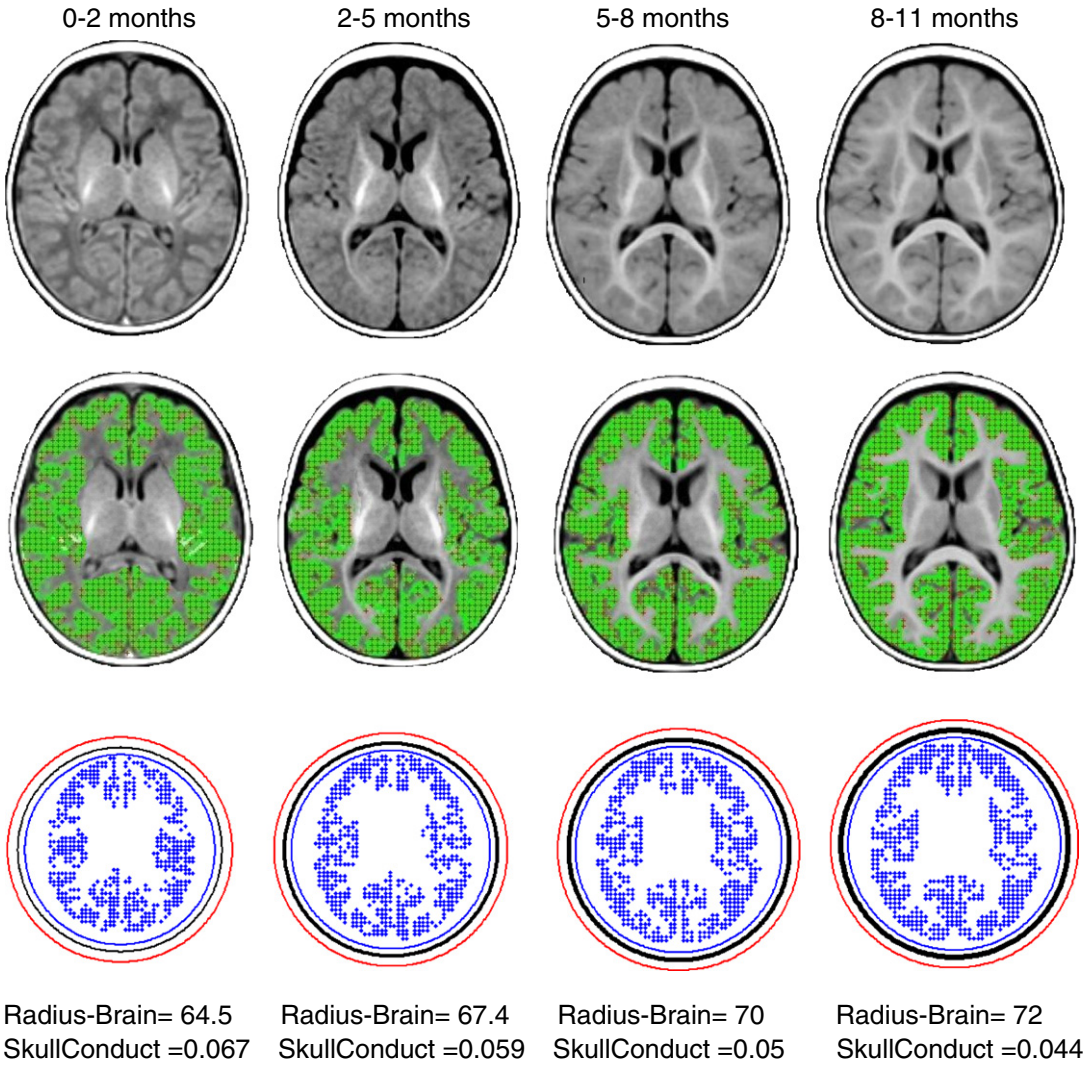

Fig. 1. Neonates Brain Templates. Representative slices of the MNI age dependent brain MRI templates for infants. A) The upper row shows gray/white matter development with age in T1 images (Fonov templates). Note that the white-gray matter intensities in the 0–2 months' template are not clearly delimited. B) The middle row shows the gray matter segmentation defined for each template together with the grid where EEG sources are defined. C) The last row shows the spherical model adjusted for each template. The radiuses in the figure correspond to the sphere fitted to the brain cortex and it increases with age. The conductivities are the skull conductivity assumed for each template, which is decreasing with age .These basic parameters define the age dependent forward models used in source imaging.

others. This often caused outliers in the sample which are not artifactual recordings or abnormal individuals. To cope with this type of data, the alternative is to use methods that are robust to the presence of outliers. In this regard, the ordinary least squares regression is one of the worst choices.

To limit the effect of outliers, in the present paper, the regression equations were calculated by a robust regression (Huber, 1964, 1981; Huber and Ronchetti, 2009; Wager et al., 2005) using iteratively reweighted least-squares, with the bi-square weighting function. In each step new weights were computed for each point to give lower weight to points that were far from their predicted values, and the fit was repeated using these weights. The process continued until it converged. Tests for the degree of the polynomial fit, when corrected for multiple tests using the FDR criterion (see below) showed that linear regressions adequately explained the dataset.

While we have only described the regression equations for the values of log spectra, a matching set of developmental equations was obtained for the standard deviation around the mean. Values for age dependent mean and standard deviations are both necessary for Statistical Parametric Mapping as will be made clear in the next section.

SPM

The coefficients of the regression equations can be used, combined with the age and log-spectra of a new individual, to calculate the Z probabilistic transformation for every source (lead) at each frequency:

$$Z = \frac{x-\mu}{\sqrt{\sigma}},$$

where x is the value of the subject for the variable, μ and σ are respectively the mean and the variance obtained from the regression equations for the variable in consideration. As a further refinement we used the modified z score proposed by Crawford and Howell (1998) which distributes as a t statistic:

$$Z^C = \frac{x-\mu}{\sqrt{\left(\sigma^* \frac{N+1}{N}\right)}}.$$

At the leads, these values can be viewed as the topographic Z-maps. At the sources, they can be viewed as a statistical 3D Z image (Bosch-Bayard et al., 2001), with each source color-coded proportional to its

Z score. These maps and images quantify the significance of the deviation of a given lead or source from the corresponding age matched normative group. Extreme deviations from the normative values will show up as "hot spots" as has become standard in SPM.

An overall summary statistic of deviation from the norm may be obtained using multivariate methods (Huizenga et al., 2007). A simpler approach, more suited to tomographic images, is to simply count the number of voxels that exceed the FDR threshold (Benjamini and Hochberg, 1995). This global measure of abnormality shall be called the *global Z index*.

Study sampling design

The sampling design to construct normative databases must ensure a large enough sample to provide adequate statistical power for the hypothesis to be tested. In our case, compare a single subject with the normative database.

For SPM the situation is complicated by simultaneously testing a large number of highly correlated variables. Thus power calculations must be able to cope with a high number of multiple comparisons. At least two methods for power calculations in neuroimaging have been developed: 1) Hayasaka et al. (2007) developed a methodology based on non-central random field theory; and 2) Suckling et al. (2010) have proposed another alternative which is able to estimate the power quite accurately using the False Discovery Rate (FDR). In the present work, we focus on the latter (FDR) alternative.

Unlike traditional analysis that estimates the power (1-β) (type-II error rate) for a fixed significance level (α) (type-I error rate), the expected value for the FDR (q) statistic is used as a control parameter, in the following equation: (Eq. 6 in Suckling et al. (2010))

$$q = \frac{\alpha}{\alpha + \frac{\varnothing}{1-\varnothing}\phi^*\left(Z_\alpha^C - \delta/_{SE}\right)},$$

where q is the expected value of the FDR allowed for multiple testing (q = 0.1 in the present work); α is the traditional significance level (α = 0.05 in the present work); δ is the effect size that centers the distribution of the alternative hypotheses; SE is the standard deviation of the normative database; θ is the proportion of tests that belongs to the alternative distribution (θ = 0.1 in the present work) and ϕ^* is the survival function of the normal distribution; Z_α^C is the critical value for p of the Crawford corrected Z. The appropriate sample size of the normative database (N), which is implicit in the Z_α calculation, was evaluated using the above specified parameters. The resulting calculations are shown in Fig. 2. The left panel shows that the smallest effect δ detectable asymptotes to about 3.2 for sample sizes larger than 50. Using a δ of 3.4 the right panel shows that for an FDR of 0.1 the power achieved is 0.86 for the sample size of the normative database presented in this paper.

ROC analysis of the global z index

To test sensitivity and specificity of the normative database (with the global z index as a classification score) a cross validated receiver operator characteristic (ROC) technique was used. A sample of 17 neonates (9 from the Institute of Neurobiology in Queretaro, Mexico and 8 from the "Juan Manuel Marquez" Pediatric Hospital in Havana, Cuba) with different history of brain damage (hypoxia, convulsive crisis, brain infarct, myoclonic epilepsy and others) was taken as the pathological group. Seventeen randomly chosen subjects were then removed from the normative sample and the age dependent topographic and tomographic regression equations were obtained with the remaining 76 normal subjects as a training set. This assured an unbiased evaluation of the normal subjects.

A summarizing ROC curve for the global z index was based on the 17 patients and a 17 normal test set. This procedure was repeated 10 times, randomly selecting the 17 subjects of the normal test sample in each trial. The ten ROC curves were then averaged. As a general index for diagnostic accuracy we retained the area under the ROC curve (AUC) at a specificity of 0.15. This is a general measure of diagnostic accuracy that is independent of the specific threshold for classification (Obuchowski, 2006).

Results and discussion

Topographic regression equations of EEG spectra with age

Our prior paper (Otero et al., 2011) described regression equations for topographic Broad Band Spectral Parameters (BBSP), for three EEG montages: linked ears, laplacian and average reference. In this paper we present the more detailed Narrow Band Spectral Parameter equations (Szava et al., 1994). Additionally we extend the frequency range studied to 50 Hz, up from the 19 Hz of our prior work.

In general agreement with the above cited paper, we found that the Log Spectral Power in all EEG neonates pooled over age is concentrated in the slow frequency range (from 0.78 to 7.5 Hz), showing a decrease with frequency with an approximate 1/f shape, as can be seen in Fig. 3. Fig. 4 illustrates the topographic distribution of EEG power (pooled over age) for selected bands. There is a clear anterior–posterior increase with a superimposed area of power increase at Cz from 0.78 to 18 Hz.

A different way to analyze the topographic regression developmental equations is to look at the *rates of change* of spectral power. For this purpose, t-tests were used to assess the significance of the robust regression coefficients at all leads and frequencies. These tests were thresholded with a correction for multiple comparisons setting the global False Discovery Rate at q = 0.05 (Benjamini and Hochberg, 1995). We thus can obtain a topographic t-map for the rate of change of log spectral power with age. Stacking the maps for all frequencies yields a 3D image that summarizes the significant changes of EEG power with age (Fig. 5).

Several features are evident from Fig. 5. In the first place, there is striking left/right symmetry of regression slopes. Moreover, power changes with age are concentrated to only certain frequency bands—there is no change for 12.5–19 Hz (low-Beta band) and 32–45 Hz (middle-Gamma). There is a marked decrease for slower frequencies, widespread over all leads for delta with a concentration in frontal leads for theta and alpha. This decrease is mirrored in high Gamma (45–50 Hz) with concentration in frontal regions that spread out to the all leads with higher frequencies. In contrast, power increased sharply with age from 19 to 32 Hz, except in frontal leads, changes being more evident at central, parietal and temporal leads than at occipital ones.

Summarizing these scalp EEG findings, they provide greater spatial and frequency detail than those previously reported by our group

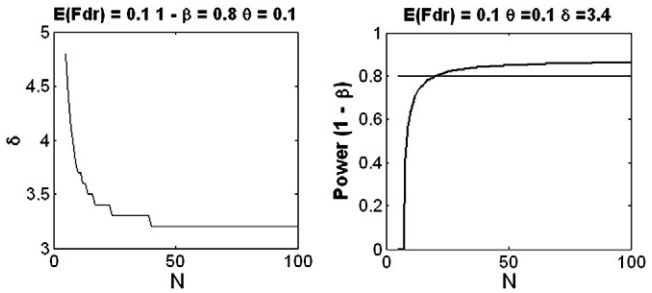

Fig. 2. Power calculations for normative databases. Power for normative studies dependence on sample size. Parameters that remain fixed are displayed in the corresponding title. Left panel: Minimum effect size of the alternative distribution vs. the normative database sample size for a fixed power of (1-β). Right Panel: Power vs. sample size of the normative database. All curves have the expected FDR (E(Fdr) in the figure title) controlled at q = 0.1.

—in effect dissecting the topographic features of frequency specific changes that were previously lumped together in Otero et al. (2011). In particular in the theta band it is evident that age dependent changes for 3.5 Hz are widespread, whereas those at 7.5 are quite localized. While we have reported only results for the average reference EEG montage, similar regression equations were obtained for other montages including the laplacian.

How are the developmental changes in EEG topographic power reflected at the sources? This will be dealt with in the next section.

Tomographic regression equations of EEG spectra with age

The behavior of the mean Log spectra at the sources was similar to the one observed for power spectra at the leads. Fig. 6 illustrates this characteristic at the sources; note the correspondence with Fig. 5. In Fig. 6, each cut in the YZ plane is a sagittal view of the maximum intensity plot (MIP) of the *t*-test (threshold with the global FDR corrected threshold) at all sources, created for a specific frequency. The lower panel is a 2D (ZX) projection of the same image to facilitate visual inspection of the frequencies where significant age related changes took place.

By frequency bands, the observed changes are very similar to the results at the leads, except in the Alpha band, where no source exceeded the threshold.

Condensing such amount of information in just one figure is illustrative but some details are missed. For example, in the Delta band, the sources near the vertex were not significant, same as at the leads, where Cz was not significant. In the temporal poles greater values for the slow frequencies were observed up to 6 months of age compared to occipital and parietal cortices. These results are interesting since in our knowledge they have not been previously reported.

The greater amplitude of the slow frequencies in the temporal lobes of infants up to 6 months is a finding difficult to explain. As in the log power spectra the general tendency of the log current spectra in these frequencies is to decrease with age. These results, as the results of the log power spectra are in agreement with previous reports in the literature by visual inspection of the EEG (Otero, 2001) and by quantitative analysis (Hagne et al., 1973; Otero et al., 2011).

The Log Spectra at the sources in frequencies between 7.5 and 19 Hz showed higher values in the low alpha band in the occipital regions and lower values were in orbito-frontal regions. In the temporal regions a progressive increase in the Log spectra values with increasing age was observed. In dorsal frontal and parietal regions no major changes with age were apparent. The Log Spectra at the sources in high-Beta and low-Gamma frequencies had an important increase with age in all explored regions between 19 and 32 Hz approximately. Our findings in relation to the Log Spectra at the sources

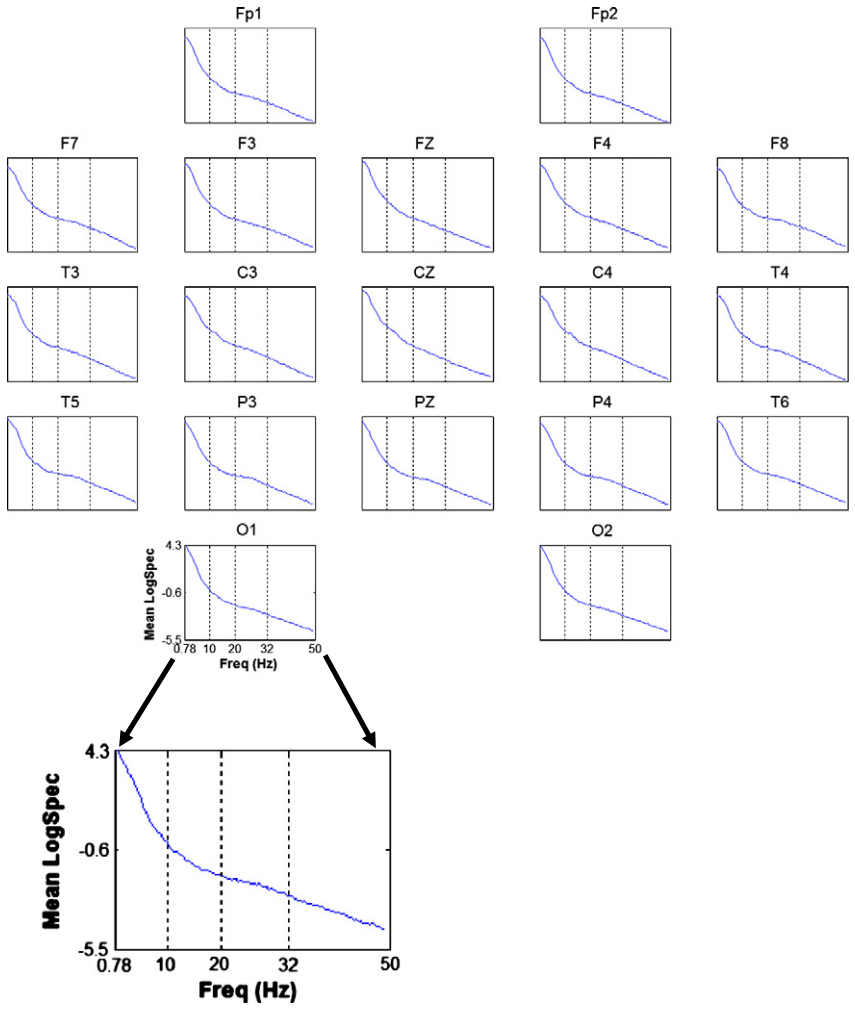

Fig. 3. Age pooled mean log spectrum. The mean Log Spectrum (Y-axis) pooling over the age range, for each lead from 0.78 to 50 Hz (X-axis). Slow activity (078 to 7.5 Hz) predominates. Note there is an anterior/posterior gradient with increase in the posterior leads (the Log spectra in the posterior leads reach the maximum values).

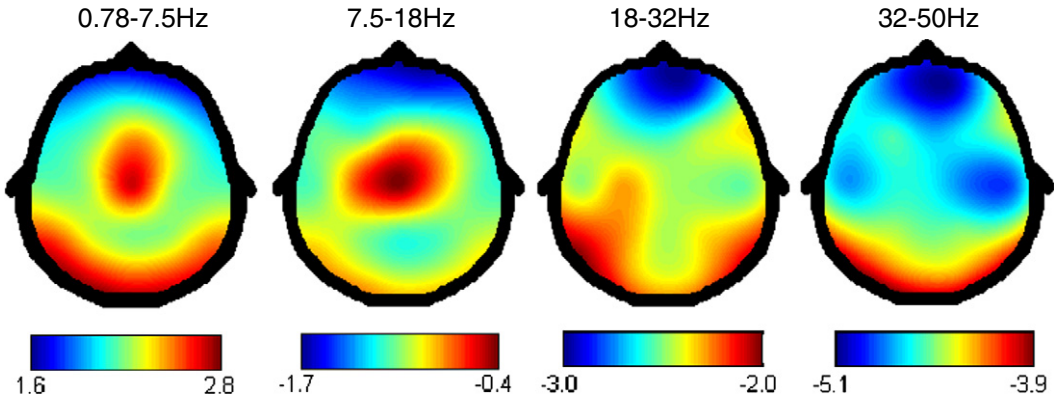

Fig. 4. Topographic distribution of age pooled mean log spectrum at selected frequencies. Scalp topographic maps showing the anterior/posterior gradient of the Log Spectra mean for all ages at selected frequency ranges. From left to right: 0.78–7.5 Hz, 7.5–18 Hz, 18–32 Hz and 32–50 Hz. Note that the gradient peripheral to Cz does not appear at frequencies higher than 18 Hz. There is an increment of the power log spectra at the parietal leads from 18 to 32 Hz.

in the studied frequencies during the first year of age have important developmental implications. For the first time it has been evident across this range of age the differences in EEG maturation between different cortical regions in a frequency range from 0.78 to 50 Hz. It has been also shown the development of oscillations at higher frequencies as high-Beta and low-Gamma that play an important role in cognition.

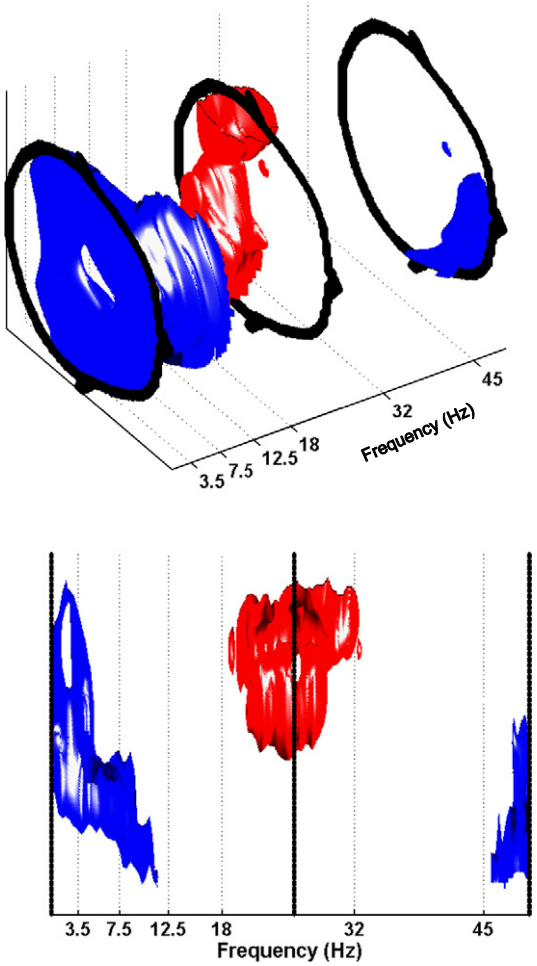

Fig. 5. Regression slopes for topographic EEG log spectra. Upper panel: 3D map showing the significant *t*-test results for regression slopes of all leads and frequencies from 0.78 to 50 Hz (X-axis). Each cut in the ZY plane is a topographic map (seen from above) of all t tests for a specific frequency. Only t-values exceeding the global FDR corrected threshold (2.46) are shown. The lower panel is a 2D view of the above image, showing the specific frequencies where the regressions were most significant. Blue codes for a decrease with age, while red color an increase.

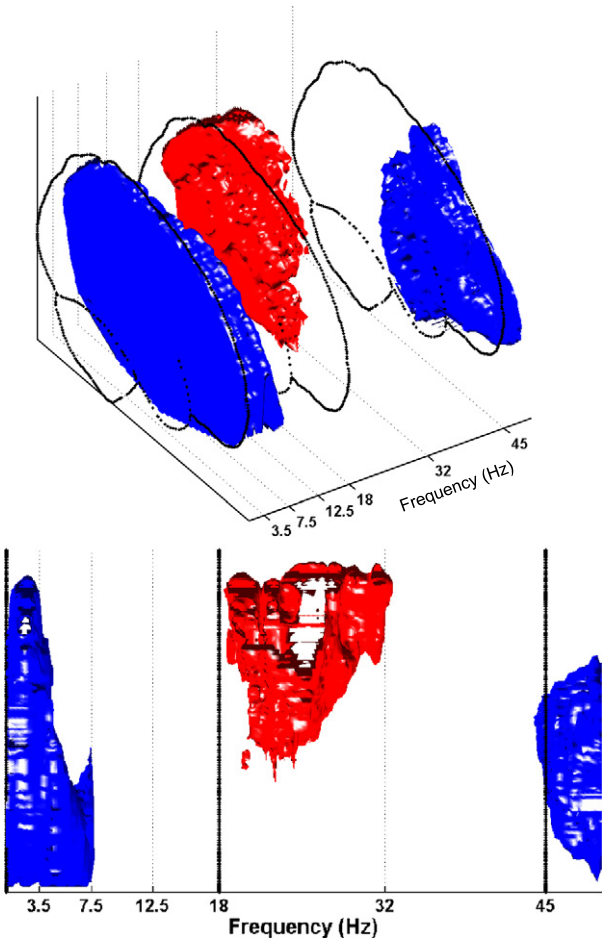

Fig. 6. Regression slopes for tomographic sources log spectra. Upper panel: 3D map showing the significant *t*-test results for the regression of all sources and frequencies from 0.78 to 50 Hz (X-axis). A sagittal maximum intensity (MIP) plot is shown in each ZX cut at a specific frequency. Only t-values exceeding the global FDR corrected threshold (3.49) are shown. The lower panel is a 2D view of the above image, showing the specific frequencies where the regressions were significant. Blue codes a decrease with age, while red codes an increase. Note that these results are in agreement with the findings at the leads (Fig. 5).

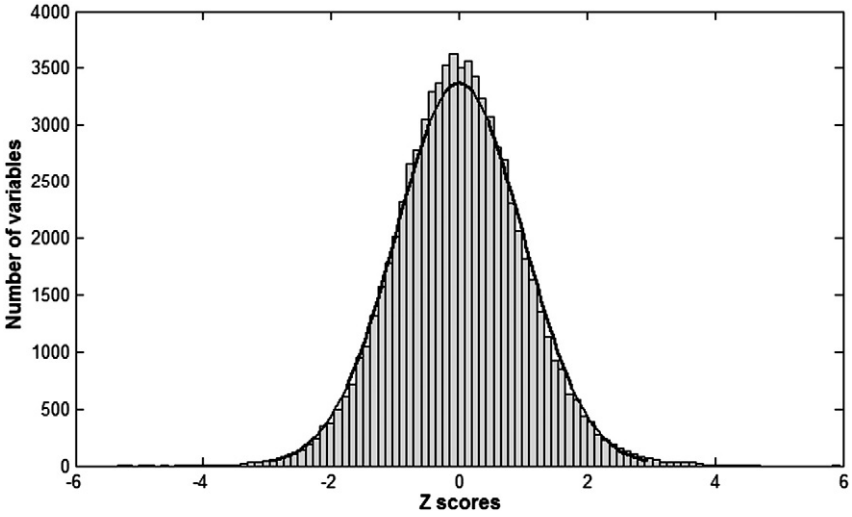

Fig. 7. Histogram of the cross validated Z scores for all variables and frequencies. The black line is the fitted Gaussian distribution.

Implications of topographic and tomographic regression equations

In spite of recent progress in elucidating the neural origins of different EEG rhythms (Amzica and Lopes da Silva, 2011), a direct connection of this line of work to changes in the different EEG oscillations in the human newborn and infants is not yet completely clear (Mizrahi et al., 2011; Riviello et al., 2011). Nevertheless there is abundant evidence that during the first year of life remodeling or resculpting of interconnected neural networks is very intense, since dendritic arborization, synaptogenesis, myelinization, neurotransmitter development, apoptosis and many other plastic changes evolve in an intensive and extensive manner. As argued in Scher (2008) and Ednick et al. (2009) the ontogeny of sleep (and EEG) in neonate and infants will ultimately be explained by these changes. Recent Neuroimaging studies may help test these hypotheses. For example the linear regressions described here are echoed in those published by Kuklisova-Murgasova et al. (2011) for gray and white matter. Even moreover detail is provided by Oishi et al. (2011) with a multi-contrast neonatal brain atlases showing that white matter in neonates has a decrease in Mean Diffusivity and an increase in Fractional Anisotropy for DWI with age. These changes indicate a posterior- to-anterior and a central-to-peripheral maturation of white matter consistent with the spectral changes shown in Fig. 3. Future work outside of the scope of this paper will relate these MRI morphometric measures with EEG changes along the lines initiated in Valdes-Hernandez et al. (2010).

Validation of the normative database

Specificity

Thatcher et al. (2003, 2005) have proposed standards to assess the specificity of normative databases using the empirical probability distribution of Z scores for all subjects.[2] These scores are computed by leaving each subject out and calculating the corrected z value with the respective mean and standard deviation (SD) provided by the regression equations calculated with the rest of the subjects. Z scores are pooled for all voxels and frequencies. Fig. 7 shows the histogram of the distribution of the Z scores for all variables and frequencies. The black line is the approximate Gaussian distribution.

In our study we obtained 2.53% at +2SD; 2.12% at −2SD, 0.37% at +3SD and 0.20% at −3SD, demonstrating that the specificity of the z values for our normative database is in the expected range of values with those described in Thatcher et al., 2003.

Diagnostic accuracy

Example of topographic (scalp) z maps for brain damaged infants had already been shown in Otero et al. (2011). We now present z images for normal and brain damaged infants in Figs. 8 and 9 which show substantial differences for both groups. Fig. 8 allows a panoramic view of all pathological and all normal subjects in the database. It can be seen that, while not perfect, the procedure does seem to have adequate diagnostic accuracy. Fig. 9 is a detailed rendering of z images for some of the brain damaged infants as well as for a normal subject. For one pathological case the MRI is shown with a striking correspondence of EEG source abnormalities with the MRI findings.

These qualitative impressions were then substantiated by calculating the ROC curve for the global z index as described in the Materials and methods. The highest area under the ROC curve (AUC) was that for the tomographic procedure (0.80). This is in agreement with previous results of our group reviewed in Hernandez-Gonzalez et al. (2011) that suggested that Electrophysiological Source Imaging may sharpen classification results due to the spatial deconvolution it entails. The AUC for scalp measures was much lower, 0.69 for average reference and 0.48 for the laplacian montages respectively. The disappointing results with the laplacian procedure came as a surprise in view of the expected higher spatial localization that was obtained in initial publications by our group (Pascual-Marqui et al., 1988). However they do seem to be typical of this type of data as suggested qualitatively in Otero et al. (2011) and quantitatively in Thatcher et al. (2003). We speculate that the greater spatial accuracy of the laplacian may be offset by the increase of signal to noise which may be important in infant recording.

The sensitivity and specificity achieved with 3D EEG SPM, while statistically significant certainly needs improvement. One avenue is to construct discriminant equations in which take into account not only the probability distribution of the normal sample but also that of infants with brain dysfunction. Such methods are available from the Brain Computer Interface literature (Dyrholm and Parra, 2007)

[2] Note that in Thatcher et al. (2003) the definition of sensitivity and specificity is not the usual one in Medical Statistics—we adhere to the latter.

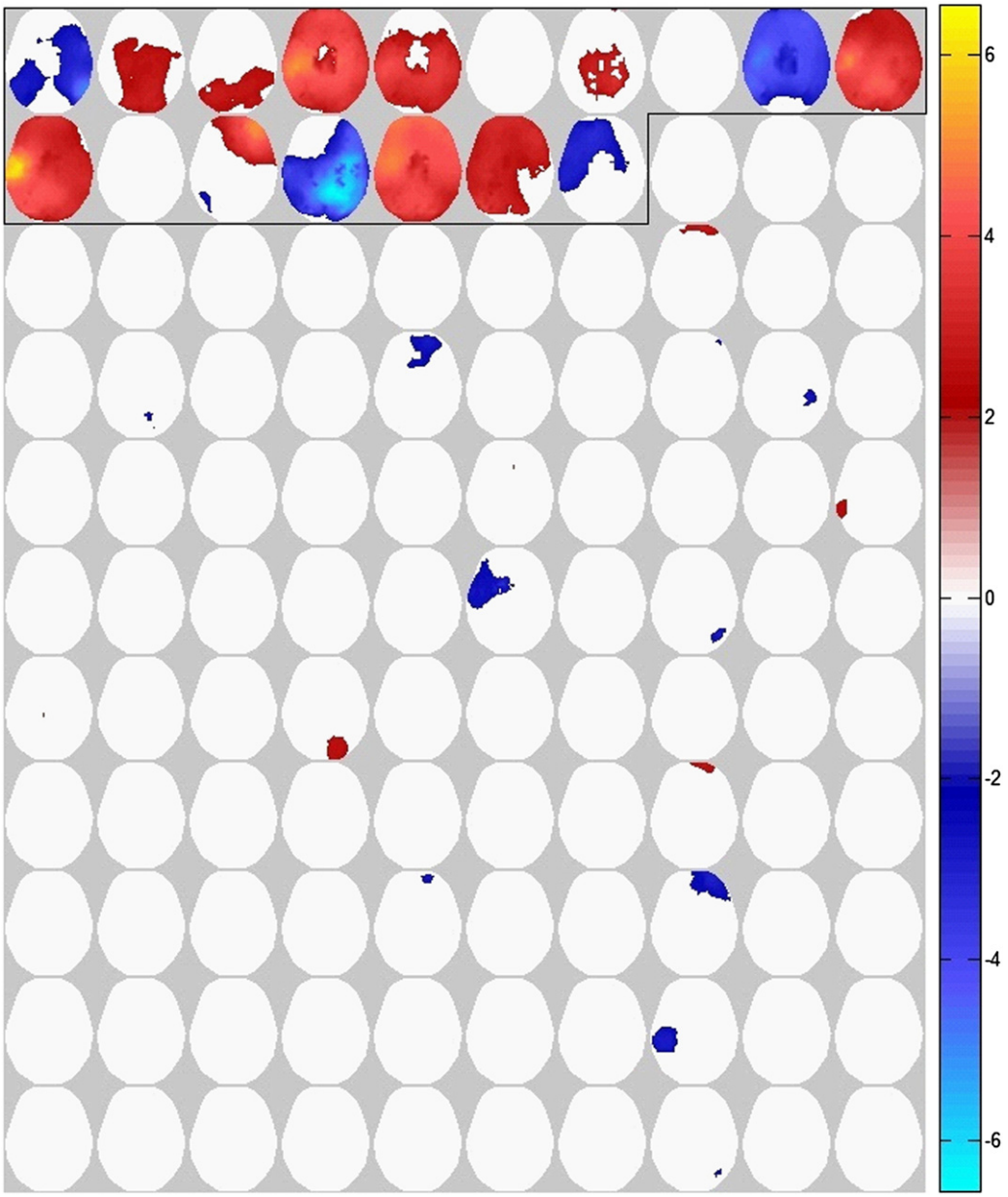

Fig. 8. MIP of Z-scores in the delta band for both normal and pathological neonates. Maximum Intensity Projection (MIP), top view, of the Z-scores for the 17 pathological neonates (top of the figure, demarked by black lines) and the 93 normal subjects at the frequency (in the Delta band) most deviant from the norm. Z-scores for normal subjects were obtained by recalculating the norms each time using the leave one out procedure. All Z-scores were thresholded to a common value of ± 2.4 SD. Two of the pathological cases only showed Z-scores above the threshold in the Beta band between 15 and 24 Hz and appear in white in this figure. The third one was included as pathological due to clinical evidence of brain damage, but with visual EEG inside normal range. This case did not show Z-scores beyond the limits in any frequency of the whole frequency range.

and from Multivoxel Pattern Analysis (Klemen and Chambers, 2012) and will be evaluated more extensively in a future paper.

Conclusions

This paper presents developmental equations for the age dependent means and standard deviations of narrow band EEG log spectral power for a normative sample of 93 neonates from age 1 to 10 months in stage 2 of sleep. This normative data is obtained for the frequency band 0.78–50 Hz for scalp data (thus extending a prior study) and for current source densities estimated with Electrical Source Imaging. The main finding from these regressions is that slow wave activity decreases with age, at lower frequencies for the whole brain, at slightly higher frequencies only in the frontal areas. This same situation is valid for 45–50 Hz, a frequency range not much studied till now. By contrast there is an increase with age in the frequency band of 19–32 Hz localized in parietal, temporal and occipital areas. The diagnostic usefulness of these regression equations is validated by ROC analysis that includes 17 neonates with brain damage. The area under the ROC curve for EEG source SPM is 0.80, for average reference scalp EEG SPM is 0.69 and for laplacian EEG SPM is 0.48—this latter technique performing essentially at chance levels. Thus, 3D Statistical Parametric Mapping of quiet sleep EEG is a promising approach for the evaluation of brain damage in the first year of life. However, the calculation of EEG normative data is particularly interesting since these norms may serve as early markers of cognitive and behavioral development. Deviations from normal EEG ontogenesis may help to discriminate high-risk infants (i.e. preterm newborns with low weight, term and preterm newborns with asphyxia, infants with infections) and to follow up their neurodevelopment.

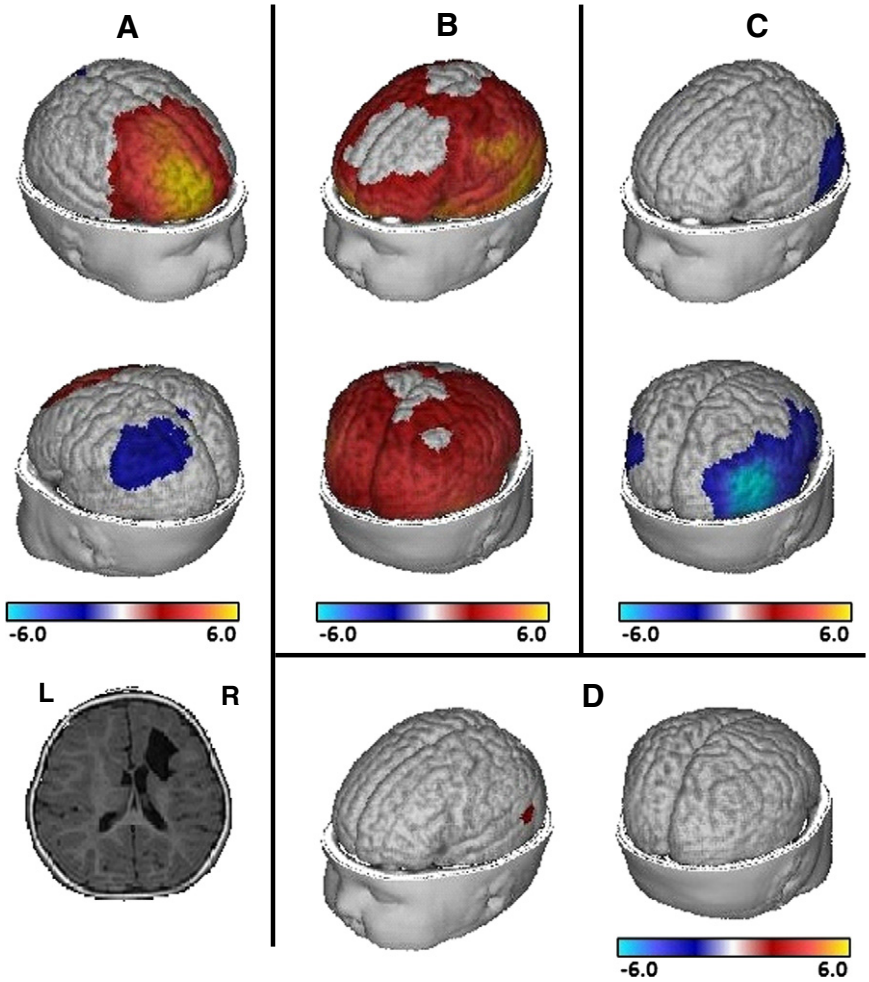

Fig. 9. Composite 3D EEG SPM of neonates. Panel A: 3D EEG SPM at 2.34 Hz of a 3 months old infant with a brain infarct of the frontal right hemisphere, occupying an extended area in the frontal area. The third row in this panel is an axial slice of the infant's T1 showing the area of the brain infarct. The corresponding tomographic 3D Z image shows an excess in the right frontal area. This pattern of pathological activity was consistent at all frequencies of the delta band (0.78–3.5 Hz). The blue color indicates a decrease of energy (minimum z-values of −2.9) in the left temporal area, which was not observed at frequencies below 1.56 Hz. Panel B: tomographic 3D Z image at 3.12 Hz of a 9 months old infant with a periventricular leukomalasia with expanded sylvian and pontine cisterns. An extended area of pathological activity was found in both hemispheres. Maximum of z-values are observed at the temporal left hemisphere. Panel C: tomographic 3D Z image at 1.95 Hz of a 2 months old infant who suffered surgery due to hydrocephaly and had a catheter implanted in the right hemisphere. Panel D: tomographic 3D Z image at 2 Hz of a normal 4 months old infant who was not a member of the normative sample.

Acknowledgments

The authors want to acknowledge the technical assistance of David Avila Acosta and M. in Sc Juan José Ortiz Retana with the acquisition of the MRI data and Salvador Ocampo and Rosa Maria Hernandez for EEG recordings at the Neurobiology Institute, UNAM campus Juriquilla.

References

Alemán-Gómez, Y., Melie-García, L., Valdés-Hernandez, P., 2006. IBASPM: toolbox for automatic parcellation of brain structures. Presented at the 12th Annual Meeting of the Organization for Human Brain Mapping, June 11–15, 2006, Florence, Italy: Available on CD-Rom in NeuroImage, vol. 27. No.1.

Alvarez, A., Valdés, P., Pascual, R., 1987. EEG developmental equation confirmed for Cuban schoolchildren. Electroencephalogr. Clin. Neurophysiol. 67, 330–332.

Amzica, F., Lopes da Silva, F.H., 2011. Cellular substrates of brain rhythms. Chapter 3 In: Schomer, D.L., Lopes da Silva, F. (Eds.), Niedermeyer's Electroencephalography: Basic Principles, Clinical Applications and Related Fields, 6th edition. Lippincott Williams and Wilkins.

Bayley, N., 1993. Bayley Scales of Infant Development, Second edition. The Psychological Corporation, San Antonio; TX USA.

Benjamini, Y., Hochberg, Y., 1995. Controlling the false discovery rate: a practical and powerfulapproach to multiple testing. J. R. Stat. Soc. B 57 (1), 289–300.

Bosch-Bayard, J., Valdes-Sosa, P., Virues-Alba, T., Aubert-Vazquez, E., John, E.R., Harmony, T., Riera-Diaz, J., Trujillo-Barreto, N., 2001. 3D statistical parametric mapping of EEG source spectra by means of variable resolution electromagnetic tomography (VARETA). Clin. EEG Neurosci. 32 (2), 47–61.

Cantor, D.S., Chabot, R., 2009. QEEG studies in the assessment and treatment of childhood disorders. Clin. EEG Neurosci. 40, 113–121.

Crawford, J.R., Howell, D.C., 1998. Comparing an individual's test score against norms derived from small samples. Clin. Neuropsychol. 12 (4), 482–486.

Darvas, F., Ermer, J.J., Mosher, J.C., Leahy, R.M., 2006. Generic head models for atlas-based EEG source analysis. Hum. Brain Mapp. 27 (2), 129–143.

Dyrholm, M., Parra, L.C., 2007. Bilinear discriminant component analysis. J. Mach. Learn. Res. 8, 1097–1111.

Ednick, M., Cohen, A.P., Mcphail, G.L., Beebe, D., Simakajornboon, N., Amin, R.S., 2009. A review of the effects of sleep during the first year of life on cognitive, psychomotor, and temperament development. Sleep (Rochester) 32 (11), 1449–1458.

Evans, A.C., Collins, D.L., Mills, S.R., Brown, E.D., Kelly, R.L., Peters, T.M., 1993. 3D statistical neuroanatomical models from 305 MRI volumes. Proceedings of IEEE-Nuclear Science Symposium and Medical Imaging Conference, 95, pp. 1813–1817.

Fenichel, G.M., 2007. Neonatal Neurology, 4th edition. Elsevier Inc.

Fernandez, T., Harmony, T., Fernandez-Bouzas, A., Díaz-Comas, L., Prado-Alcalá, R.A., Valdés-Sosa, P., Otero, G., Bosch, J., Galán, L., Santiago-Rodríguez, E., Aubert, E., García-Martínez, F., 2007. Changes in EEG current sources induced by neurofeedback in learning disabled children. An exploratory study. Appl. Psychophysiol. Biofeedback 32, 169–183.

Fernandez-Bouzas, A., Harmony, T., Galán, L., Marosi, E., Fernandez, T., Reyes, A., Silva, J., Rodríguez, M., Bernal, J., Alonso, M., 1995. Comparison of Z and multivariate statistical brain electromagnetic maps for the localization of brain lesions. Electroencephalogr. Clin. Neurophysiol. 95, 372–380.

Fernandez-Bouzas, A., Harmony, T., Fernandez, T., Ricardo, J., Casián, G., Sánchez-Conde, R., 2001. Cerebral blood flow and sources of abnormal EEG activity (VARETA) in neurocysticercosis. Clin. Neurophysiol. 112, 2281–2287.

Fonov, V., Evans, A.C., Botteron, K., Almli, C.R., McKinstry, R.C., Collins, D.L., Brain Development Cooperative Group, 2011. Unbiased average age-appropriate atlases for pediatric studies. Neuroimage 54 (1), 313–327.

Galan, L., Biscay, R., Neira, L., Virues, T., 1994. Multivariate statistical brain electromagnetic mapping. Brain Topogr. 7, 17–28.

Gevins, A.S., Remond, A. (Eds.), 1987. Handbook of Electroencephalography and Clinical Neurophysiology. Elsevier Science Publishers B.V., Amsterdam.

Gordon, E., Cooper, N., Rennie, C., Hermens, D., Williams, L.M., 2005. EEG integrative neuroscience: the role of a standardized database. Clin. EEG Neurosci. 36, 64–75.

Hagne, I., Persson, J., Magnusson, R., Petersén, I., 1973. Spectral analysis via fast Fourier transform of waking EEG in normal infants. In: Kellaway, P., Petersen, I. (Eds.), Automation of Clinical Electroencehalography. Raven Press, New York, pp. 103–144.

Harmony, T., Marosi, E., Díaz de León, A.E., Becker, J., Fernandez, T., 1990. Effect of sex, psychosocial disadvantages and biological risk factors on EEG maturation. Electroencephalogr. Clin. Neurophysiol. 75, 482–491.

Harmony, T., Fernandez-Bouzas, A., Marosi, E., Fernandez, T., Bernal, J., Rodríguez, M., Reyes, A., Silva, J., Alonso, M., Casián, G., 1993. Correlation between computed tomography and voltage and current source density spectral EEG parameters in patients with brain lesions. Electroencephalogr. Clin. Neurophysiol. 87, 196-20xz5.

Hayasaka, S., Peiffer, A.M., Hugenschmidt, C.E., Laurienti, P.J., 2007. Power and sample size calculation for neuroimaging studies by non-central random field theory. Neuroimage 37, 721–730.

Hellström-Westas, L., de Vries, L.S., Rosén, I., 2008. An Atlas of Amplitude-Integrated EEGs in the Newborn, 2nd edition. Informa Healthcare, London, United Kingdom.

Hernandez, J.L., Valdes, P., Biscay, R., Virues, T., Bosch, J., Riquenes, A., Clark, I., 1994. A global scale factor in brain topography. Int. J. Neurosci. 76 (3–4), 267–278.

Hernandez-Gonzalez, G., Bringas-Vega, M.L., Galan-Garcia, L., Bosch-Bayard, J., Lorenzo-Ceballos, Y., Melie-Garcia, L., Valdes-Urrutia, L., Cobas-Ruiz, M., Valdes-Sosa, P., 2011. Multimodal Quantitative Neuroimaging Databases and Methods the Cuban Human Brain Mapping Project. Clin. EEG Neurosci. 42 (3), 149–159.

Homma, S., Musha, T., Nakajima, Y., Okamoto, Y., Blom, S., Flink, R., Hagbarth, K.E., 1995. Conductivity ratios of the scalp-skull-brain head model in estimating equivalent dipole sources in human brain. Neurosci. Res. 22 (1), 51–55.

Huber, P.J., 1964. Robust estimation of a location parameter. Ann. Math. Stat. 35, 73–101.

Huber, P., 1981. Robust Statistics. John Wiley and Sons, New York.

Huber, P., Ronchetti, E.M., 2009. Robust Statistics, 2nd edition. John Wiley and Sons, New York.

Huizenga, H.M., Smeeding, H., Grasman, R.P.P.P., Schmand, B., 2007. Multivariate normative comparisons. Neuropsychologia 45, 2534–2542.

Hunter, M., Smith, R.L., Hyslop, W., Rosso, O.A., Gerlach, R., Rostas, J.A., et al., 2005. The Australian EEG database. Clin. EEG Neurosci. 36, 76–81.

John, E.R., Karmel, B.Z., Corning, W.C., Easton, P., Brown, D., Ahn, H., John, M., Harmony, T., Prichep, L., Toro, A., Gerson, I., Bartlett, P., Thatcher, R., Kaye, H., Valdés, P., Schwartz, E., 1977. Neurometrics. Science 196, 1393–1410.

John, E.R., Ahn, H., Prichep, L., Trepetin, M., Brown, D., Kaye, H., 1980. Developmental equations for the electroencephalogram. Science 210, 1255–1258.

John, E.R., Prichep, L.S., Easton, P., 1987. Normative data banks and neurometrics. Basic concepts, methods and results of norms construction. In: Gevins, A.S., Remond, A. (Eds.), Handbook of Electroencephalography and Clinical Neurophysiology, vol. I. Elsevier Science Publishers B.V., Amsterdam, pp. 449–495.

Joseph, J.P., Lesevre, N., Dreyfus-Brisac, C., 1976. Spatiotemporal organization of EEG in premature infants and full-term new-borns. Electroencephalogr. Clin. Neurophysiol. 40, 153–168.

Klemen, J., Chambers, C.D., 2012. Current perspectives and methods in studying neural mechanisms of multisensory interactions. Neurosci. Biobehav. Rev. 36 (1), 111–133.

Korotchikova, S., Connolly, C.A., Ryan, D.M., Murray, A., Temko, B.R. Greene, Boylana, G.B., 2009. EEG in the healthy term newborn within 12 hours of birth. Clin. Neurophysiol. 120, 1046–1053.

Kuklisova-Murgasova, M., Aljabar, P., Srinivasan, L., Counsell, S.J., Doria, V., Serag, A., Gousias, I.S., et al., 2011. A dynamic 4D probabilistic atlas of the developing brain. Neuroimage 54 (4), 2750–2763. doi:10.1016/j.neuroimage.2010.10.019 Elsevier Inc..

Lai, Y., Van Drongelen, W., Ding, L., Hecox, K.E., Towle, V.L., Frim, D.M., He, B., 2005. Estimation of in vivo human brain-to-skull conductivity ratio from simultaneous extra- and intra-cranial electrical potential recordings. Clin. Neurophysiol. 116 (2), 456–465.

Lehmann, D., Faber, P.L., Gianotti, L.R., Kochi, K., Pascual-Marqui, R.D., 2006. Coherence and phase locking in the scalp EEG and between LORETA model sources, and microstates as putative mechanisms of brain temporo-spatial functional organization. J. Physiol. Paris 99, 29–36.

Lutkenhoner, B., Greenblatt, R., Hamalainen, M.S., et al., 2000. Comparison between different approaches to the biomagnetic inverse problem: workshop report. In: Aine, C.J., Okada, Y., Stroink, J., Swithenby, S.J., Wood, C.C. (Eds.), Biomag 96: Proceedings of the Tenth International Conference on Biomagnetism. Springer Verlag.

Mandelbaum, D.E., Krawciw, N., Assing, E., Ostfeld, B., Washburn, D., Rosenfeld, D., et al., 2000. Topographic mapping of brain potentials in the newborn infant: the establishment of normal values and utility in assessing infants with neurological injury. Acta Paediatr. 89, 1104–1110.

Matousek, M., Petersén, I., 1973. Frequency analysis of the EEG in normal children and adolescents. In: Kellaway, P., Petersén, I. (Eds.), Automation of Clinical Electroencephalography. Raven Press, New York, pp. 75–102.

Michel, C., Murray, M., Lantz, G., Gonzalez, S., Spinelli, L., Grave de Peralta, R., 2004. EEG source imaging. Clin. Neurophysiol. 115, 2195–2222.

Michel, Christoph M., Koenig, Thomas, Brandeis, Daniel, Gianoti, Lorena R.R., et al., 2009. Electrical Neuroimaging. Cambridge University Press.

Mizrahi, E.M., Moshé, S.L., Hrachovy, R.A., 2011. Normal EEG and sleep: preterm and term neonates: chapter 9, In: Schomer, D.L., Lopes da Silva, F. (Eds.), Niedermeyer's Electroencephalography: Basic Principles, Clinical Applications and Related Fields, 6th edition. Lippincott Williams and Wilkins, pp. 164–182.

Niemarkt, H.J., Andriessen, P., Peters, C.H., Pasman, J.W., Blanco, C.E., Zimmermann, L.J., Bambang-Oetomo, S., 2010. Quantitative analysis of amplitude-integrated electroencephalogram patterns in stable preterm infants, with normal neurological development at one year. Neonatology 97 (2), 175–182.

Obuchowski, N.A., 2006. An ROC-type measure of diagnostic accuracy when the gold standard is continuous-scale. Stat. Med. 481–493. doi:10.1002/sim.2228 September 2004.

Oishi, K., Mori, S., Donohue, P.K., Ernst, T., Anderson, L., Buchthal, S., Faria, A., et al., 2011. Multi-contrast human neonatal brain atlas: application to normal neonate development analysis. Neuroimage 56, 8–20. doi:10.1016/j.neuroimage.2011.01.051 Elsevier Inc.

Okumura, A., Kubota, T., Tsuji, T., Kato, T., Hayakawa, F., Watanabe, K., 2006. Amplitude spectral analysis of theta/alpha/beta waves in preterm infants. Pediatr. Neurol. 34, 30–34.

Oostendorp, T.F., Delbeke, J., Stegeman, D.F., 2000. The conductivity of the human skull: results of in vivo and in vitro measurements. IEEE Trans. Biomed. Eng. 47 (11), 1487–1492 Nov.

Otero, G., 2001. Ontogenia y maduración del electroencefalograma. In: Alcaraz, V.M., Guma, E. (Eds.), Texto de neurociencias cognitivas. Manual Moderno, México DF, pp. 371–394.

Otero, G.A., Harmony, T., Pliego-Rivero, F.B., Ricardo-Garcell, J., Bosch-Bayard, J., Porcayo-Mercado, R., Fernandez-Bouzas, A., Díaz-Comas, L., Galán, L., Vieyra-Reyes, P., Fernandez, T., 2011. QEEG norms for the first year of life. Early Hum. Dev. 87, 691–703.

Pascual-Marqui, R.D., 2002. Standardized low resolution brain electromagnetic tomography (sLORETA): technical details. Methods Find. Exp. Clin. Pharmacol. 24D, 5–12.

Pascual-Marqui, R., Gonzalez, S., Valdes-Sosa, P., 1988. Current source density estimations and interpretation based on the spherical harmonic Fourier expansion. J. Neurosci. 43.

Pascual-Marqui, R.D., Michel, C.M., Lehmann, D., 1994. Low resolution electromagnetic tomography: a new method for localizing electrical activity in the brain. Int. J. Psychophysiol. 18, 49–65.

Pascual-Marqui, R.D., Lehmann, D., Koenig, T., Kochi, K., Merlo, M.C.G., Hell, D., Koukkou, M., 1999. Low resolution brain electromagnetic tomography (LORETA) functional imaging in acute, neuroleptic-naive, first-episode, productive schizophrenia. Psychiatry Res. 90, 169–179.

Paul, K., Krajca, V., Roth, Z., Melichar, J., Petránek, S., 2006. Quantitative topographic differentiation of the neonatal. Clin. Neurophysiol. 117, 2050–2058.

Ricardo-Garcell, J., González-Olvera, J.J., Miranda, E., Harmony, T., Reyes, E., Almeida, L.G., Galán, L., Díaz-Comas, L., Ramírez, L., Fernandez-Bouzas, A., 2009. EEG sources in a group of patients with major depressive disorder. Int. J. Psychophysiol. 71, 70–74.

Riera, J.J., Aubert, E., Valdés, P., Casanova, R., Lins, O., 1996. Discrete spline electric-magnetic tomography (DSPET) based on realistic neuronatomy. In: Wood, C. (Ed.), Proceedings of The Tenth International Conference on Biomagnetism, BIOMAG'96, Santa Fe, New Mexico.

Riviello, J.J., Nordli, D.L., Niedermeyer, E., 2011. Normal EEG and sleep: infants to adolescents. Chapter 10 In: Schomer, D.L., Lopes da Silva, F. (Eds.), Niedermeyer's Electroencephalography: Basic Principles, Clinical Applications and Related Fields, 6th edition. Lippincott Williams and Wilkins, pp. 164–182.

Rush, S., Driscoll, D.A., 1968. Current distribution in the brain from surface electrodes. Anesth. Analg. 47, 717–723.

Scher, M., 2005. Electroencephalography of the newborn: normal and abnormal features. In: Niedermeyer, E., Lopes da Silva, F. (Eds.), Electroencephalography, Basic Principles, Clinical Application and Related Fields. Williams & Wilkins, USA.

Scher, M.S., 2008. Ontogeny of EEG-sleep from neonatal through infancy periods. Sleep Med. 9 (6), 615–636. doi:10.1016/j.sleep. 2007.08.014.

Schomer, D.L., Lopes da Silva, F. (Eds.), 2011. Niedermeyer's Electroencephalography: Basic Principles, Clinical Applications and Related Fields, 6th edition. Lippincott Williams and Wilkins, pp. 164–182.

Sekihara, Kensuke, Nagarajan, Srikatan S., 2008. Adaptive Spatial Filters for Electromagnetic Brain Imaging. Springer.

Suckling, J., Barnes, A., Job, D., Brenan, D., Lymer, K., Dazzan, P., Marques, T.R., MacKay, C., McKie, S., Williams, S.R., Williams, S.C.R., Lawrie, S., Deakin, B., 2010. Power calculations for multicenter imaging studies controlled by the false discovery rate. Hum. Brain Mapp. 31, 1183–1195.

Szava, S., Valdés, P., Biscay, R., Galán, L., Bosch, J., Clark, I., Jiménez, J.C., 1994. High resolution quantitative EEG analysis. Brain Topogr. 6, 211–219.

Thatcher, R.W., Walker, R.A., Guidice, S., 1987. Human cerebral hemispheres develop at different rates and ages. Science 236, 1110–1113.

Thatcher, R.W., Walker, R.A., Biver, C.J., North, D., Curtin, R., 2003. Sensitivity and specificity of the Neuroguide EEG normative database: validation and clinical correlation. J. Neurother. 7 (3/4), 87–121.

Thatcher, R.W., North, D., Biver, C., 2005. Evaluation and validity of a LORETA normative EEG database. Clin. EEG Neurosci. 36 (2), 116–122 Apr.

Valdes, P., Valdés, M., Carballo, J.A., Alvarez, A., Díaz, G.F., Biscay, R., Pêrez, M.C., Szava, S., Virués, T., Quesada, M.E., 1992. QEEG in a public health system. Brain Topogr. 4, 259–266.

Valdes-Hernandez, P., von Ellenrieder, N., Ojeda-Gonzalez, A., Kochen, S., Alemán-Gómez, Y., Muravchik, C., Valdés-Sosa, P.A., 2009. Approximate average head models for EEG source imaging. J. Neurosci. Methods 185 (1), 125–132. doi:10.1016/j.jneumeth.2009.09.005.

Valdes-Hernandez, P.A., Ojeda-Gonzalez, A., Martinez-Montes, E., Lage-Castellanos, A., Virues-Alba, T., Valdes-Urrutia, L., Valdes-Sosa, P.A., 2010. White matter architecture rather than cortical surface area correlates with the EEG alpha rhythm. Neuroimage 49, 2328–2339. doi:10.1016/j.neuroimage.2009.10.030 Elsevier Inc.

Valdes-Sosa, P.A., Vega, M., Sanchez, J.M., Martinez, E., Bobes, M., 2009. EEG source imaging with spatio temporal tomographic nonnegative independent component analysis. Hum. Brain Mapp. 30, 1898–1910.

Victor, S., Appleton, R.E., Beirne, M., Marson, A.G., Weindling, M., 2005. Spectral analysis of electroencephalography in premature newborn infants: normal ranges. Pediatr. Res. 57, 336–341.

Wager, T.D., Keller, M.C., Lacey, S.C., Jonides, J., 2005. Increased sensitivity in neuroimaging analyses using robust regression. Neuroimage 26, 99–113.

West, C.R., Harding, J.E., Williams, C.E., Gunning, M.I., Battin, M.R., 2006. Quantitative electroencephalographic patterns in normal preterm infants over the first week after birth. Early Hum. Dev. 82, 43–51.

Willekens, H., Dumermuth, G., Duc, G., Mieth, D., 1984. EEG spectral power and coherence analysis in healthy full-term neonates. Neuropediatrics 15, 180–190.